Preparation and Performance Analysis of New Multi stage Porous Carbon Materials for Air Pollution Treatment

Pingli ZHANG [1] *, **Zhenyu YANG** [2], **Baosheng MU** [1], **Jingjing HUANG** [1], **Qianqian MA** [1], **Hongchao LI** [1], **Jia JIA** [3]

[1] *Department of Land Information and Management, Henan College of Surveying and Mapping, Zhengzhou, 450015, China*
[2] *Department of Computer Engineering, Henan College of Surveying and Mapping, Zhengzhou, 450015, China*
[3] *Department of Space Information Engineering, Henan College of Surveying and Mapping, Zhengzhou, 450015, China*

The adsorption of toxic and harmful gases through porous materials is an effective means of air pollution control. A multi-level porous carbon material with ultra-high-specific surface area was made based on rice husk biomass to improve the air pollution controlling efficiency and reduce its cost. The rice husk substrate was pretreated using *T.viride* spore suspension during the preparation of this material. This changes the proportion of various components in the matrix, thereby achieving an increase in the multi-level porous carbon material's specific surface area. Its performance was analyzed through various means in the study. The results confirmed that when the activation treatment time was 60 minutes, the porous carbon material's specific surface area was the highest, reaching 3714 m^2/g. After 30 days of treatment with *T.viride* spore suspension, the cellulose content in rice husks decreased by about 40 g/kg. Compared to untreated porous carbon materials, after 20 days of treatment, the micropores and mesopores of these materials significantly increased. The research has successfully increased the multi-level porous carbon material's specific surface area and achieved rapid absorption of atmospheric volatile organic compounds. The multi-level porous carbon material can enhance the air pollution controlling efficiency and reduce its cost.

Keywords: carbon neutrality, multi-level porous carbon, air pollution, VOCs, *T.viride*.

1. INTRODUCTION

Air pollution becomes an increasingly serious problem with the acceleration of global industrialization, especially in rapidly industrializing developing countries. The emissions of harmful substances such as particulate matter, sulfur dioxide, and nitrogen oxides cause serious impacts on the environment and public health. With the increasing challenges of global climate change, countries are actively seeking response strategies. Air pollution is a type of environmental pollution that is difficult to treat. As a core means of controlling air pollution, pollution adsorption technology has always been highly efficient and cost-effective [1]. Traditional adsorption materials, due to their limited adsorption capacity and selectivity, are difficult to meet the requirements of high efficiency and low-cost air purifying [2]. The Multi-Level Porous Carbon (MLPC) materials have provided new possibilities for improving adsorption efficiency and optimizing usage costs [3]. This new material exhibits excellent performance in the adsorption of atmospheric pollutants due to its multi-level pore structure, high Specific Surface Area (SSA), and adjustable pore size, especially in the adsorption of some small molecule pollutants [4]. However, MLPC materials' SSA has reached the bottleneck period, making it difficult to continue generating MLPC materials with higher SSA levels. This study proposes to use microorganisms to treat biomass matrix materials to improve the efficiency of air pollution treatment and reduce the cost of air pollution treatment. Meanwhile, multi-stage Porous Carbon Materials (PCMs) are prepared using the pre-treated biomass matrix.

The study innovatively proposes the use of fungi to treat the material matrix and change the proportion of various substances, thereby increasing the material's SSA. The research contribution lies with a high-performance MLPC material based on a rice husk matrix, which has been used to achieve an increase in atmospheric Volatile Organic Compounds (VOCs) absorption efficiency.

2. RELATED WORKS

The SSA of multi-stage PCMs directly affects their adsorption efficiency for VOCs. Huang, X. et al. proposed using pine towers as a biomass carbon source to improve the electromagnetic wave absorption performance. The tower was combined with hydrothermal and pyrolysis methods to prepare porous carbon composite materials. Meanwhile, the effect of the cerium source on the electromagnetic parameters of the composite materials was studied. The results showed that the composite material had excellent electromagnetic wave absorption ability, which was expected to provide new solutions for electromagnetic interference and pollution treatment [5]. Yu, Z. et al. designed graded porous hollow carbon nanospheres with radially arranged support ribs to improve the performance of lithium sulfur batteries and solve the sulfur injection and utilization. This structure not only maximized the injection and utilization of sulfur, but also enhanced electronic conductivity. The results showed that the material exhibited

---

* Corresponding author. Tel.: +86-0371-5666-2017.
E-mail: *150017@hasm.edu.cn* (P. Zhang)

good capacity and cycling performance after nitrogen doping [6]. Wei, X. et al. proposed a method for preparing cross-linked polyphosphazene nanospheres with tunable hollow structures. Hexachlorocyclophosphazene and tannic acid were used as co-monomers, and a substitutable third co-monomer was introduced. The results showed that N/P doped mesoporous carbon nanospheres were obtained after carbonization, exhibiting excellent oxygen reduction reaction performance [7]. Ren et al. reviewed the composition, structure, and synthesis methods of inorganic organic hybrid crystal derived carbon materials in energy storage to explore their potential applications. The results showed that inorganic organic hybrid crystal derived carbon had advantages such as large SSA, porous structure, and heteroatom doping. Meanwhile, this substance has shown great potential in rechargeable lithium/sodium ion batteries, lithium-sulfur batteries, supercapacitors, and other fields [8]. Air pollution treatment is currently the main research direction in environmental protection. Khatib, M. et al. introduced the basic knowledge and sensing methods of VOCs sensing to summarize the latest developments in the field of VOCs sensors. The main trends in material design were proposed, with a particular focus on nanostructures and nanohybridization. The results showed that emerging sensing materials and strategies showed wide applications and potential in different types of sensing technologies [9]. Weisskopf, L. et al. investigated the diversity of microbial volatile compounds and their functions in interbiological interactions. The chemical diversity of microbial volatiles and their mechanisms were proposed for mediating rapid chemical interactions. The results showed that microbial volatiles played an important role in the interactions between microorganisms, plants, and insects. Meanwhile, these volatiles had potential applications in biotechnology [10]. Gu, S. et al. estimated the ozone formation potential (OFP) and SOA formation potential of anthropogenic and biogenic VOCs to evaluate the role of VOCs in ozone and Secondary Organic Aerosol (SOA) production. The anthropogenic VOCs and related industries that dominated OFP and SOA, as well as the potential impact of urban greening on air quality were proposed. The results indicated that vegetation types with low VOCs emissions needed to be considered to avoid deterioration of air quality [11]. In summary, VOCs are a type of air pollution that is currently difficult to treat and poses significant harm to human health. Activated carbon adsorption is currently an effective method for treating volatile gas pollution. Meanwhile, the efficiency of activated carbon adsorption treatment is directly related to the SSA of the activated carbon material. Therefore, a method for preparing activated carbon materials using microbial treatment is proposed to improve the treatment efficiency of activated carbon materials for VOCs pollution and reduce treatment costs.

3. MATERIALS AND METHODS

3.1. Examination devices and materials

MLPC prepared in this experiment is based on a biomass matrix. Meanwhile, the matrix material used is rice husk. Other experimental materials include *T.viride* freeze-dried powder, potato culture medium, potassium hydroxide, copper ethylenediamine, nitrogen, toluene standard gas, m-xylene standard gas lotus leaf carbon AC-x, and mesoporous lotus leaf carbon PCAC-x. Table 1 shows the main instruments and equipment used in this experiment.

Table 1. Experimental installation

Name	Type	Name	Type
Electronic weight scale	BWS-15-N	Vibration incubator	DHZ-LA
Vacuum oven	DHG-9055AD	Mass flow meter	D08-4C/ZM
Analytical balance	BSA124S	Gas chromatograph	GC-2014C
Tube furnace	OTF-1200X	Vacuum pump	SHZ-DIII
Raman spectrometer	LabRAM Aramis	X-ray powder diffractometer	D8A Dvance
High resolution transmission electron microscope	FEI f20	High resolution field emission scanning electron microscope	Merlin
Micromeritics	ASAP-2020	Adsorption evaluation reaction device	–
IGA	IGA-100	Nuclear magnetic resonance	AVANCE III 400
Tg-ms	STA449 F3	x-ray photoelectron spectroscopy	Escalab 250xi

3.2. Preparation of multi-level porous carbon

Before preparing MLPC, spore suspension needs to be prepared. Meanwhile, the production of spore suspension needs to be kept sterile throughout the process. The production steps of *T.viride* spore suspension are as follows. Dilute *T.viride* freeze-dried powder by 10000 times with pure water until completely dissolved. Take freeze-dried powder solution and inoculate it into the culture medium. Incubate at a constant temperature of 28 °C until many normal colonies grow on the culture medium. Add pure water dropwise to the culture medium, scrape out the fungi from the medium, and filter them. Transfer the bacterial solution into a conical flask and make up to volume. Spore suspensions need to be sealed and stored at 6 °C in a refrigerator [12, 13]. The rice husk's main components include cellulose, lignin, silica, and hemicellulose. It has a good MLPC framework and is an excellent biological matrix material for VOCs adsorption treatment. However, due to the influence of the proportion of basic components in rice husks, synthesizing MLPC materials with ultra-high SSA using rice husks as substrates is difficult [14, 15]. Fungal pretreatment can target the decomposition of components in the biological matrix to make the proportion of cellulose, hemicellulose, and other components in the biomass matrix changed, achieving the preparation of ultra-high SSA MLPC.

The rice husk pretreatment fungus used is *T.viride*. Fig. 1 shows the route for synthesizing MLPC materials through biological pretreatment. The MLPC material prepared is high-performance rice husk MLPC, and the preparation steps are as follows. Clean the rice husks with pure water and dry them for later use. Add potato culture medium, pure water, and rice husks to a large conical flask, and shake until fully dissolved.
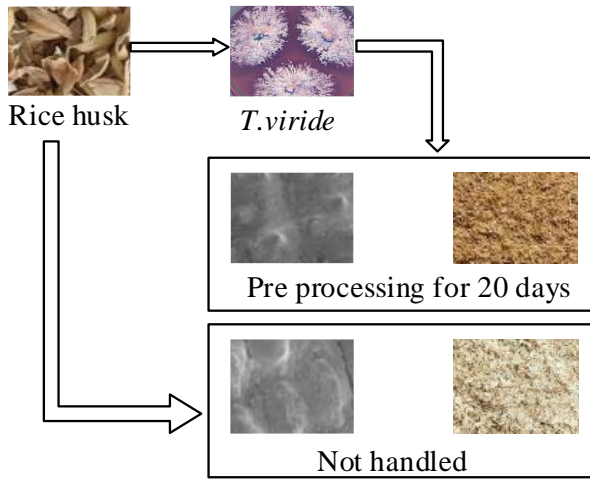
Fig. 1. Biological pretreatment route for synthesizing multi-level porous carbon materials

Drip *T.viride* spore suspension into the rice husk solution and incubate at 28 °C and 140 r/min in the incubator. After completing the modification, rinse with clean water and dry in an 80 °C oven for 12 hours. Place the dried sample in a 100 ml/min environment, raise the temperature to 600 °C at a rate of 5 °C/min, and carbonize for 60 minutes. After carbonization is completed, mix and grind the carbonized sample with potassium hydroxide according to the activation ratio. Place the sample in a tube furnace and raise its temperature to the activation temperature at a heating rate of 5 °C/min to activate the sample after thorough grinding and mixing. After activation, rinse the sample with pure water to neutralize and dry it in an 80 °C oven for 12 hours to obtain rice husk MLPC [16, 17].

3.3. Experimental setup design

A dynamic adsorption evaluation device for VOCs is designed to analyze the adsorption effect of MLPC on VOCs. The device consists of MLPC adsorption, gas supply, and gas chromatography analysis systems. The dynamic adsorption evaluation of the device is divided into four steps, namely standard gas testing, loading VOCs adsorption of MLPC materials, and evaluation of adsorption capacity. Before the adsorption of VOCs, it should increase the concentration of VOCs to a fixed concentration and evacuate the device gas before opening the gas path at the sample loading position. The sample reaches adsorption saturation when the concentration of VOCs in the gas chromatography test rises to the standard gas concentration and the VOCs concentration at the outlet remains unchanged. Fig. 2 shows the dynamic adsorption evaluation device designed for research.

In the designed adsorption evaluation equipment, the arrow indicates the gas direction in the device. Standard gas is used to test the adsorption evaluation. Then PCM is loaded into the adsorption tube. When the VOCs concentration is stable, the sample gas path is opened until the VOCs concentration rises to the standard concentration. When using this device for gas chromatography analysis, it is necessary to adjust the electric constant temperature box

to 25 °C. The amount of multi-stage PCM is $0.02 - 0.1$ g. $\varphi 6$ quartz tubes are used to hold the multi-stage PCM.
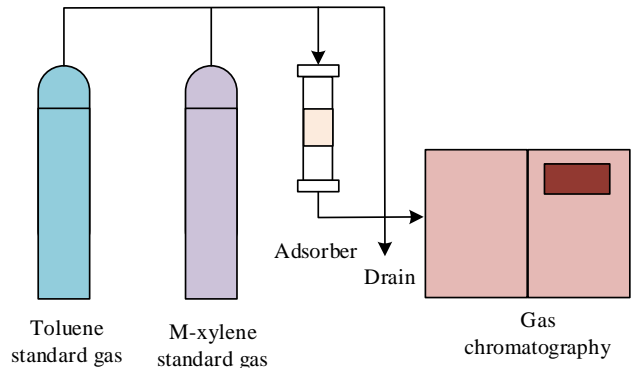

Fig. 2. Dynamic adsorption evaluation device

3.4. Evaluation of adsorption performance

The experiment evaluates the sample's adsorption performance with the dynamic adsorption device shown in Fig. 2. Eq. 1 is the calculation of VOCs' dynamic adsorption capacity in the sample [18, 19].

$$q = \frac{FC_0 10^{-9}}{W} \left[t_s - \int_0^{t_s} \frac{C_i}{C_0} dt \right],$$ (1)

where q represents VOCs' maximum adsorption capacity per unit mass of adsorbent, g/g; F refers to the total gas flow rate, mL/min; C_i means VOCs' concentration at the outlet after adsorbing for i minutes, mg/m³; C_0 is the concentration of VOCs at the inlet, mg/m³; W refers to the adsorbent's mass, g; t means adsorption time, min; t_s represents the adsorption saturation time, min. The adsorption selectivity of MLPC materials is evaluated using the adsorption solution theory and calculated using the Langmuir Freundlich equation, represented by Eq. 2 [20].

$$b = b_c \frac{k_c p^{\frac{1}{n_c}}}{1 + k_c p} + b_i \frac{k_f p^{\frac{1}{n_f}}}{1 + k_f p},$$ (2)

where b_c, b_f, k_c, k_f are all parameters; c and f represent different adsorption sites; p refers to system pressure; b is the total adsorption capacity. The penetration curve of the adsorbent is simulated using the Thomas model, represented by Eq. 3 [21].

$$\frac{C}{C_0} = \frac{1}{1 + \exp\left(\frac{K_T gm}{Q} - K_T C_{0t} \right)},$$ (3)

where C represents the VOC concentration at the outlet, mg/mL; K_T refers to the Thomas model's rate constant, mL/(min·min⁻¹); g means the estimated maximum adsorption capacity, mg/g; Q means flow rate, mL/min. The diffusion coefficient of MLPC material is studied using an intelligent weight analyzer for constant pressure adsorption tests, represented by chemical diffusion coefficient and expressed by Eq. 4 [22].

$$1 - \frac{M_t}{M_{\text{inf}}} = \frac{8}{\pi^2} \exp\left(-\frac{D\pi^2 t}{4l^2}\right), \tag{4}$$

where M_t represents the mass at the moment, mg; M_{inf} refers to the mass in an equilibrium state, mg; l means half the thickness of the sample, mm; D is the chemical diffusion coefficient, cm^2/s. The degree of polymerization of MLPC materials can be expressed by viscosity. When measuring the viscosity of the material, magnetic stirring is used to completely dissolve cellulose in copper ethylenediamine solution, a 0.05 M cellulose-copper ethylenediamine solution is prepared. Then the reading is measured using a viscometer. The crystallization index reflects the influence of basic material properties and is calculated using Eq. 5 [23].

$$C_r I = \frac{I_{002} - I_{atm}}{I_{002}} \times 100\%, \tag{5}$$

where C_r represents the crystallization index; I_{002} is the maximum peak diffraction intensity of $2\theta = 22°$; I_{atm} refers to the diffraction peak intensity of $2\theta = 18°$.

4. RESULTS AND DISCUSSION

4.1. Physical performance analysis of multi-level porous carbon materials

Four different MLPC materials were prepared based on the pre-treatment time of fungi. They are PCMs without fungal pretreatment, and PCMs with fungal pretreatment for 10, 20, and 30 days.

To analyze the effect of fungal treatment time on PCMs' SSA and pore structure, a comparative study was conducted. This study involved the nitrogen adsorbing and desorbing results of these four materials mentioned above. Four materials' pore size distribution was calculated in Fig. 3. Fig. 3 a presents the nitrogen adsorbing and desorbing curves of four materials.

As the relative pressure enhanced, the adsorbing capacity of nitrogen for each material remained elevated. When the relative pressure was less than 0.4 P/P$_0$, the adsorbing capacity of PCMs for nitrogen increased rapidly. As the relative pressure continued to increase, the adsorption capacity of PCMs for nitrogen decreased. The adsorbing effect of PCMs treated with fungi for 20 days was the best, reaching around 1400 cm^3/g·STP. As the fungal treatment time increased, the adsorbing effect of PCMs first increased and then decreased. Fig. 3 b shows the pore size distribution of four materials. The pore widths of PCMs were mostly concentrated between 1 nm and 10 nm, with a small portion having pore widths less than 1 nm. Compared to PCMs that had not been treated with fungi, other PCMs had richer pore structures. After 10 and 20 days of fungal pretreatment, the microporous structure with a volume of about 2 nm ~ 4 nm significantly increased. The increase of medium volume micropores helps to increase the SSA of PCMs, increase the adsorption sites of PCMs for VOCs, and improve the adsorption efficiency of PCMs for VOCs. RHPC-20 was studied as the object to further analyze the effect of different activation times on the structure of PCMs.
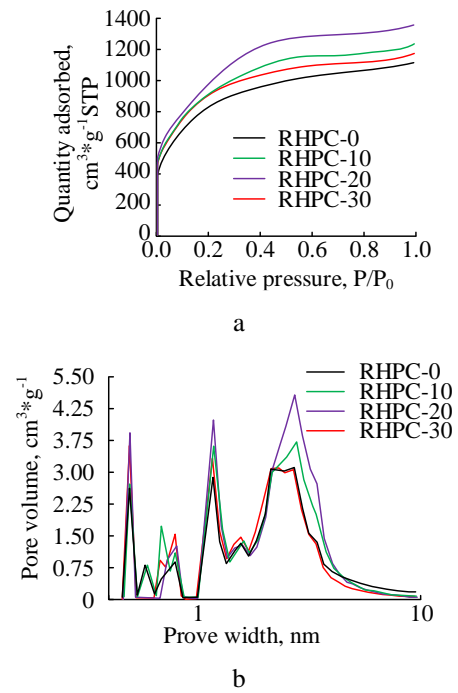
a

b

Fig. 3. a – the nitrogen adsorption-desorption curve of the four adsorption materials; b – the pore size distribution of the four adsorption materials. RHPC-0: No preprocessing is performed; RHPC-10: *T.viride* spore suspension treated for 10 days; RHPC-20: *T.viride* spore suspension was treated for 20 days; RHPC-30: *T.viride* spore suspension was treated for 30 days

The SSA and pore structure of PCMs were analyzed under different activation times in Table 2. In Table 2, when the activation treatment time was 60 minutes, the SSA of PCM was the highest, reaching 3714 m^2/g.

Table 2. Effect of activation time on porous carbon materials' specific surface area and pore structure

Time, min	APD, nm	Smic, m^2/g	SBET, m^2/g	Vmic, m^2/g	Vtot, cm^3/g
50	2.09	2104	2866	0.92	1.45
55	2.18	2089	3508	0.98	1.87
60	2.24	2028	3714	1.05	2.07
65	2.23	2249	3589	1.03	1.96
70	2.22	2316	3466	1.02	1.82
APD: average aperture; Smic: specific surface area of micropores; SBET: specific surface area; Vmic: micro-pore volume; Vtot: total pore volume.					

When the activation treatment time was 50 and 70 minutes, the SSA of the PCM was 2866 m^2/g and 3466 m^2/g, respectively. The variation of microporous SSA was opposite to that of SSA. When the activation time was 60 minutes, the microporous SSA of the material was only 2028 m^2/g. When the activation time was 50 minutes, the material's microporous SSA was 2104 m^2/g. When the activation time was 70 minutes, the material's microporous SSA was 2316 m^2/g. The micro-pore volume and total pore volume of the material showed a trend of first increasing and then decreasing with the increase of activation treatment time. When the activation time was 50 minutes, the material's micropore volume was only 0.92 cm^3/g. When the activation time was 60 min, the material's micropore volume was 1.05 cm^3/g. When the activation time was

70 minutes, the material's micropore volume was 1.02 cm³/g.

The changes in the content of cellulose, hemicellulose, and lignin in rice husks under different treatment times were studied to analyze the effect of *T.viride* spore suspension on the structure of rice husks in Fig. 4. Fig. 4 a shows the content changes of various components in rice husk MLPC material. The content of hemicellulose and lignin in rice husks remains unchanged. Meanwhile, the hemicellulose content consistently maintained at around 170 g/kg and lignin content was consistently maintained at around 185 g/kg. When not treated with *T.viride* spore suspension, rice husks' cellulose was around 330 g/kg. As the processing time increased, it continuously decreased. After 30 days of *T.viride* spore suspension treatment, it decreased to about 290 g/kg, a total decrease of about 40 g/kg. Fig. 4 b shows the C-spectrum changes of carbon materials without *T.viride* spore suspension treatment and after 20 days of *T.viride* spore suspension treatment. Two materials showed characteristic peaks at 55, 62, 72, and 104 ppm. 55 ppm corresponded to methanol lignin, 62 ppm corresponded to the crystalline region of C6 cellulose, 72 ppm corresponded to C2, C3, C5 cellulose, and 104 ppm corresponded to C1 cellulose. Compared to carbon materials without *T.viride* spore suspension treatment, the peak area of carbon materials treated with *T.viride* spore suspension for 20 days was lower. In Fig. 4 b, the cellulose change of MLPC material was consistent with the cellulose change measured in Fig. 4 a.
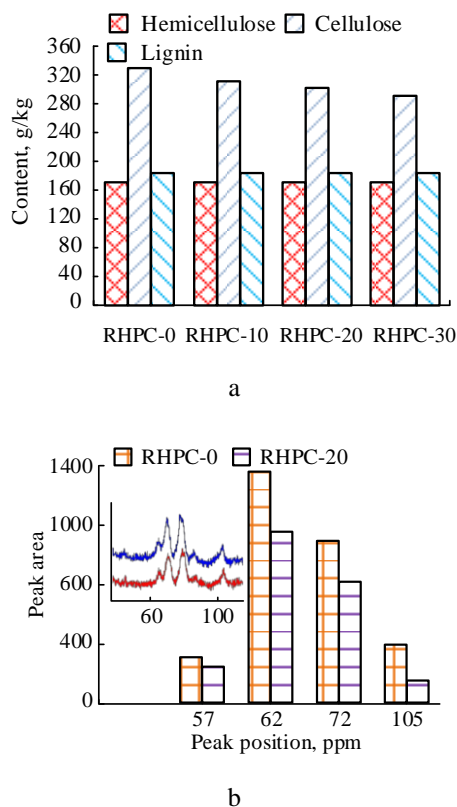

a

b

Fig. 4. Changes in cellulose, hemicellulose, and lignin content in rice husks under different processing times

Fig. 4 a shows the changes of each component in rice husks with treatment time, while Fig. 4 b shows the C-spectrum results of RHPC-0 and RHPC-20.

4.2. Microstructural analysis of multi-level porous carbon materials

The microstructure of rice husks treated with *T.viride* spore suspension was analyzed using scanning electron microscopy in Fig. 5. Fig. 5 a shows the untreated rice husks' internal structure. Fig. 5 b refers to the structure treated for 10 days. Fig. 5 c indicates the structure treated for 20 days. Fig. 5 d shows the structure treated for 30 days. The inner back of rice husks without *T.viride* spore suspension treatment had a smooth planar structure. Pores began to appear on the inner back of the rice husk after treatment with *T.viride* spore suspension. As the processing time increased, the smooth structure on the inner back of the rice husk began to show texture.

In addition to scanning electron microscopy, the structural changes of untreated and *T.viride* spore suspension treated PCMs for 20 days were analyzed using transmission electron microscopy in Fig. 6. Fig. 6 a shows the PCM without *T.viride* spore suspension treatment.
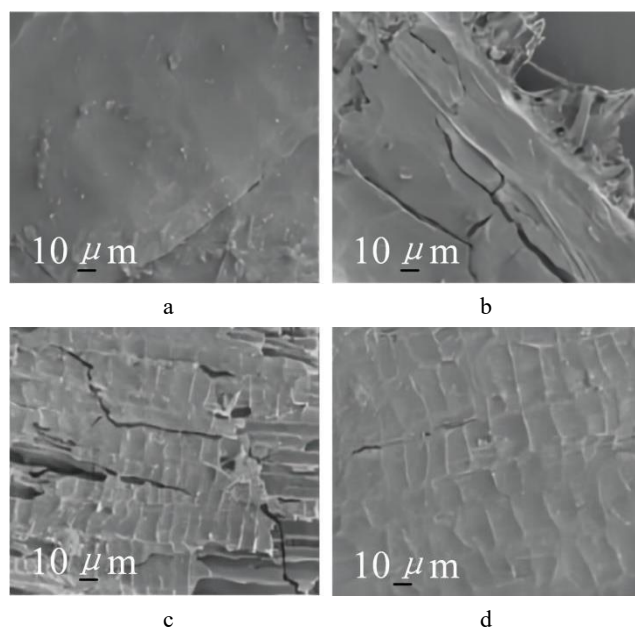

Fig. 5. SEM image of the internal structure of rice husks: a – RHPC-0; b – RHPC-10; c – RHPC-20; d – RHPC-30
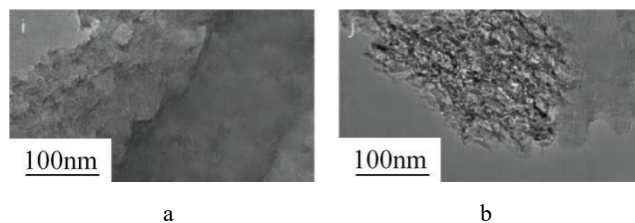

Fig. 6. TEM images of the internal structure of RHPC-0 and RHPC-20: a – RHPC-0; b – RHPC-20

Fig. 6 b means the PCM treated with *T.viride* spore suspension for 20 days. Compared to untreated PCMs, the micropores and mesopores of PCMs significantly increased after 20 days of treatment. The detection results were consistent with those in Fig. 3 b and Fig. 5. The reduction of cellulose content effectively increased the micropores and pore structure in PCMs, thereby increasing the material's SSA and increasing the absorption sites of VOCs. This

achieves the goal of improving the VOCs absorption efficiency of PCMs.

The structural properties of the prepared MLPC material were further analyzed. The material's crystallinity and surface defect degree were analyzed using X-ray diffraction, X-ray photoelectron spectroscopy, and Raman spectroscopy in Fig. 7. Fig. 7 a presents the X-ray diffraction results of MLPC material. Materials that had not been treated with *T.viride* spore suspension showed no clear broad peaks at 20° ~ 30°, but clear broad peaks at 40° ~ 50°. The broad peaks of MLPC material treated with *T.viride* spore suspension disappeared at 20° ~ 30° and 40° ~ 50° after 20 days. Fig. 7 b presented MLPC material's X-ray photoelectron spectroscopy results. The C1s spectrum of PCMs contained three component peaks. In each sample, the proportion of the three functional groups was the same. The content of sp^2 carbon and C-O groups was higher, while the content of O=C-O groups was lower. Fig. 7 c presents MLPC material's Raman spectra. All four samples exhibited two characteristic carbon peaks. The first carbon peak was located in the 1340 cm^{-1} band. The second carbon peak was located in the 1580 cm^{-1} band. The first carbon peak corresponded to the material's disordered carbon structure. The second carbon peak corresponded to the vibration frequency of graphite in the plane. The ratio of the first carbon peak's intensity to the second carbon peak's intensity for materials that had not been treated with *T.viride* spore suspension was 1.79. The ratio of materials treated with *T.viride* spore suspension for 10 days was 3.64. The ratio of materials treated for 20 days was 4.62. The ratio of materials treated for 30 days was 3.60.

4.3. Analysis of toluene adsorption effect of multi-level PCMs

To analyze the effect of the MLPC material on the adsorption performance of toluene, in Fig. 8, the toluene penetration curve of the MLPC material was analyzed. Untreated and *T.viride* spore suspension treated materials for 20 days were used. Fig. 8 a shows two MLPC materials' toluene penetration curves. The basic penetration time of untreated materials was 240 minutes. The penetration time of materials treated with *T.viride* spore suspension for 20 days was 432 minutes. Fig. 8 b shows the adsorbing capacity of MLPC material under different cycle times. After two cycles, the toluene adsorption capacity of the material treated with *T.viride* spore suspension for 20 days was about 630 mg/g. The adsorption capacity of the untreated material was about 400 mg/g.

The Monte Carlo method was used to simulate and analyze the adsorption capacity of toluene on PCMs with different pore sizes in the narrow slit pore model in Fig. 9. Fig. 9 a shows two materials' adsorbing capacity differences at different pore sizes. When the average pore size was 0.6 nm, two materials' adsorbing capacity difference was the smallest, with a difference of about - 35 mg/g. When the average pore size was 2.5 nm, two materials' adsorbing capacity difference was the largest, with a difference of about 92 mg/g. The number of pores and adsorption capacity of the material were comprehensively considered in the experiment. Fig. 9 b shows the adsorbing energy of PCMs for toluene under different pore sizes.
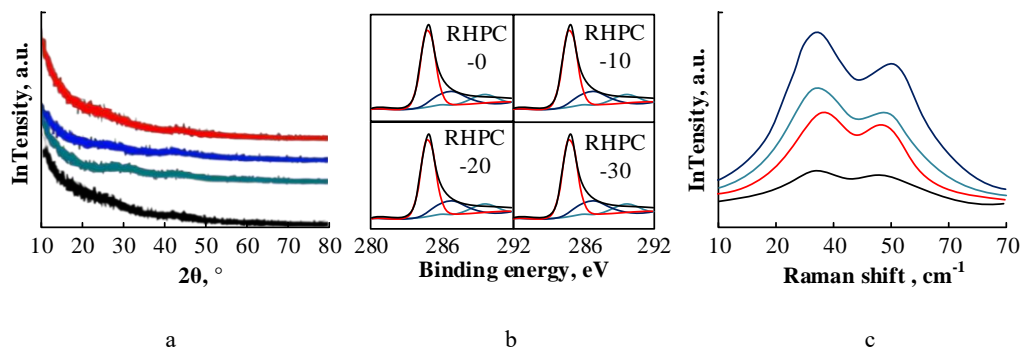

Fig. 7. Analysis of the four materials crystallinity and surface defect degree: a – XRD; b – XPS; c – Raman spectra
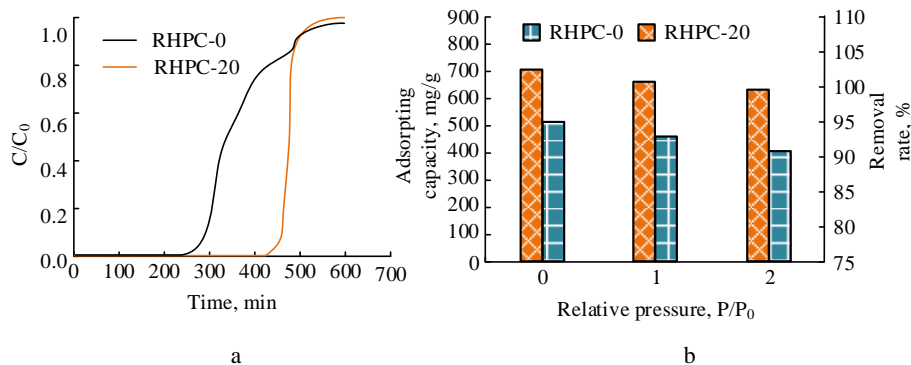

Fig. 8. a – the toluene penetration curves of two multi-level porous carbon materials; b – the adsorption capacity of two multi-level porous carbon materials in different cycles
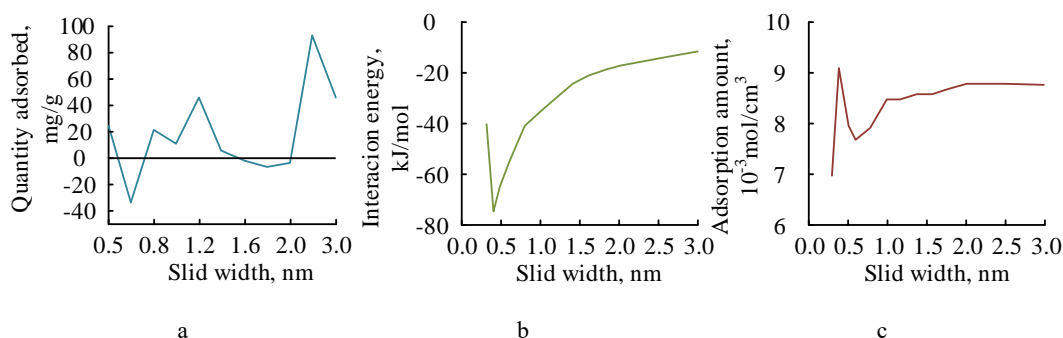
Fig. 9. Dynamic adsorption analysis of toluene of two materials: a – the adsorption difference in different pores; b – adsorption energy under different aperture; c – adsorption capacity under different pores

When the pore size was 0.4 nm, the adsorption energy of the material reached its minimum value of 74.45 kJ/mol. Then the energy gradually increased with the increase of pore size. Fig. 9 c shows the adsorption capacity at different pore sizes. When the pore size was 0.4 nm, the adsorption capacity of the material reached the highest value of $9.127 \cdot 10^{-3}$ mol/cm^3. As the fungal pre-treatment time increased, the degree of cellulose wall damage in the biomass matrix gradually increased. This led to the destruction of the structure of the prepared activated carbon material itself. The increase in pore width led to a decrease in adsorption capacity.

To further analyze MLPC materials' adsorbing characteristics, dynamic simulation analysis was conducted on untreated materials and materials treated with *T.viride* spore suspension for 20 days in Fig. 10. Fig. 10 a shows the adsorbing isotherms of toluene vapor and nitrogen on the material treated with *T.viride* spore suspension for 20 days at 293 K.
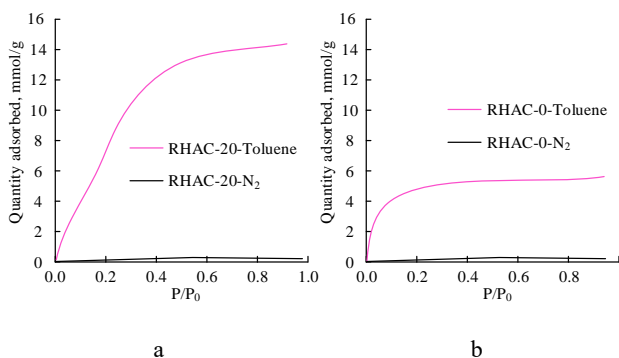

Fig. 10. Analysis of adsorption selection for multi-level porous carbon materials

This material's adsorbing capacity for toluene was much higher than that of nitrogen. When the relative pressure between toluene and nitrogen was less than 0.4, this material's adsorbing capacity for toluene increased rapidly, from 0 mmol/g to about 12 mmol/g. When the relative pressure was greater than 0.4, the adsorption capacity of the material for toluene still showed a slow upward trend. The adsorption capacity of this material for nitrogen only changed slightly with the increase of relative pressure, which could be considered unchanged. Fig. 10 b shows the adsorption isotherms of toluene vapor and nitrogen on the untreated material at 293 K. When the relative pressure was

around 0.1, this material's adsorbing capacity for toluene was basically saturated, at around 5 mmol/g. As the relative pressure continued to increase, this material's adsorbing capacity for toluene increased to around 5.8 mmol/g. The adsorption selection of nitrogen for this material was consistent with that of the material treated with *T.viride* spore suspension for 20 days. The priority was given to the absorption of VOCs such as toluene. However, the adsorption effect of the material treated with *T.viride* spore suspension for 20 days was much higher than that of the untreated material.

4.4. Discussion

Rice husk is a common biomass substrate resource. Scholars have confirmed that activated carbon materials prepared from rice husks as substrates have a high SSA [24]. The larger the SSA, the stronger the structure's ability to handle pollutants. However, the currently prepared activated carbon materials still cannot meet the requirements of air pollution control [25]. The activated carbon material's SSA can be increased by pre-treatment of the matrix material. However, the cost of preparing ultra-high SSA MLPC materials through this method is relatively high currently. Bolan N et al. found that the pore structure of MLPC materials was related to the proportion of cellulose and other components in the matrix material [26]. However, the way Bolan N et al. processed MLPC material matrices was still not the original method and required a significant amount of time and cost. Anfar Z et al. found that different microorganisms had different processing abilities for different components in biological matrix materials [27]. *T.viride* is a fungus that targets cellulose and can degrade cellulose in biomass matrix materials. Therefore, the study assumes that the rice husk biomass matrix, after being treated with *T.viride*, can change the skeleton structure of the rice husk in a short period of time. Meanwhile, the matrix can reduce the preparation cost of MLPC materials and achieve cost control of air pollution control.

The experiment explored the effect of *T.viride* fungal pretreatment on the structural properties of MLPC materials. The results confirmed that after one cycle, the toluene adsorption capacity of the material treated with *T.viride* spore suspension for 20 days was about 670 mg/g. The untreated material's adsorbing capacity was about 460 mg/g. The adsorption capacity of the material treated with *T.viride* spore suspension for 20 days was about

166 mg/g higher than that of the untreated material. This confirmed that *T.viride* fungi could destroy the structure of cellulose walls in biomass materials, while having little effect on hemicellulose, lignin, and other substances in biomass materials. The cellulose wall structure is disrupted, and the pore structure in the matrix material is increased, while other components are not affected. It can achieve an increase in MLPC materials' pore structure and SSA while maintaining their basic structure.

After *T.viride* treatment, the structure of biomass materials undergoes effective changes. After 20 days of *T.viride* treatment, the MLPC prepared from biomass matrix can reach 670 mg/g. The pore structure of PCMs prepared using this material is significantly improved. Meanwhile, the processing time is shorter, resulting in lower material processing costs. The experimental results confirm that microorganisms can change the structure of biomass matrix in a short period of time. This is consistent with Anfar Z's research results and proves the correctness of the research hypothesis.

5. CONCLUSIONS

A multi-stage PCM preparation method based on microbial pretreatment technology was proposed to improve the adsorption efficiency of PCMs for VOCs. This method utilized the destructive effect of fungi on the cellulose structure in the biomass matrix, altering the cellulose layer of the biomass matrix and increasing its pore level. The study conducted a detailed analysis of the various properties of the material through various analytical methods. The results showed that the adsorption effect of ultra-high SSA PCMs reached around 1400 cm^3/g·*STP* after 20 days of fungal treatment. When the fungal activation treatment time was 60 minutes, the SSA of the prepared material reached 3714 m^2/g. The adsorption capacity of VCOs by ultra-high SSA materials was increased by about 166 mg/g after 20 days of treatment with *T.viride* spore suspension. The main conclusions of the study are as follows:

1. Fungal treatment can effectively reduce the cellulose content in rice husks, destroy their cellulose skeleton, increase the disorder of PCMs, significantly increase the number of micropores and mesopores in the materials. Therefore, the SSA of PCMs can be increased, and an increase in the absorption efficiency of MLPC materials can be achieved;
2. When using *T.viride* spore suspension to treat microorganisms in biomass matrix, the pre-treatment time of ultra-high SSA materials can be effectively reduced and the preparation efficiency of MLPC materials with ultra-high SSA can be improved.

The research on the preparation of MLPC materials provides a new means for air pollution control. However, the activation ratio of MLPC materials was not analyzed during the preparation of this material. In the future, the activation treatment method of materials will be further improved to further reduce the preparation cost of materials and accelerate the process of air pollution control.

Nomenclature

Name	Significance	Unit
q	Maximum adsorption amount of V2OCs by unit mass adsorbent	g/g
F	Total gas flow rate	mL/min
C_i	VOCs concentration at the outlet after i minutes of adsorption	mg/m^3
C_0	VOCs concentration at the entrance	mg/m^3
W	Quality of adsorbent	g
t	Adsorption time	min
t_s	Adsorption saturation time	min
b_c, b_f, k_c, k_f	Adsorption parameters	–
c, f	Adsorption site	–
P	Systempressure	MPa
b	Total adsorption capacity	g
C	VOC concentration at the outlet	mg/mL
K_T	The rate constant of the Thomas model	mL(mg·min^{-1})
g	Estimated maximum adsorption capacity	mg/g
Q	Currentvelocity	mL/min
M_t	Mass at time t	mg
M_{inf}	Mass in equilibrium state	mg
l	Half of the sample thickness	mm
D	Chemical diffusion coefficient	cm^2/s
C_rI	Crystallization index	–
I_{002}	The maximum peak diffraction intensity of $2\theta = 22°$	–
I_{atm}	The diffraction peak intensity of $2\theta = 18°$	–

List of abbreviations

Abbreviations	Full name
MLPC	Multi-level Porous Carbon
SSA	Specific Surface Area
VOCs	Volatile Organic Compounds
PCMs	Porous Carbon Materials
SOA	Secondary Organic Aerosol
OFP	Ozone Formation Potential

REFERENCES

1. **Huang, X., Liu, X., Jia, Z., Wang, B., Wu, X., Wu, G.** Synthesis of 3D Cerium Oxide/Porous Carbon for Enhanced Electromagnetic Wave Absorption Performance *Advanced Composites and Hybrid Materials* 4 (4) 2021: pp. 1398 – 1412. https://doi.org/10.1007/s42114-021-00304-2

2. **Zheng, Y., Song, Y., Gao, T., Yan, S., Hu, H., Cao, F., Duan, Y., Zhang, X.** Lightweight and Hydrophobic Three-Dimensional Wood-Derived Anisotropic Magnetic Porous Carbon for Highly Efficient Electromagnetic Interference Shielding *ACS Applied Materials & Interfaces* 12 (36) 2020: pp. 40802 – 40814.
https://doi.org/10.1021/acsami.0c11530

3. **Liu, N., Hao, L., Zhang, B., Niu, R., Gong, J., Tang, T.** Rational Design of High-Performance Bilayer Solar Evaporator by Using Waste Polyester-Derived Porous Carbon-Coated Wood *Energy & Environmental Materials* 5 (2) 2022: pp. 617 – 626.
https://doi.org/10.1002/eem2.12199

4. **Islam, M.A., Hameed, B.H., Ahmed, M.J., Khanday, W.A., Khan, M.A., Marrakchi, F.** Porous Carbon–Based Material from Fish Scales for the Adsorption of Tetracycline Antibiotics *Biomass Conversion and Biorefinery* 13 (14) 2023: pp. 13153 – 13162.
https://doi.org/10.1007/s13399-021-02239-6

5. **Huang, X., Liu, X., Jia, Z., Wang, B., Wu, X., Wu, G.** Synthesis of 3D Cerium Oxide/Porous Carbon for Enhanced Electromagnetic Wave Absorption Performance *Advanced Composites and Hybrid Materials* 4 (4) 2021: pp. 1398 – 1412.
https://doi.org/10.1007/s42114-021-00304-2

6. **Yu, Z., Liu, M., Guo, D., Wang, J., Chen, X., Li, J., Jin, H., Yang, Z., Chen, X., Wang, S.** Radially Inwardly Aligned Hierarchical Porous Carbon for Ultra-Long-Life Lithium–Sulfur Batteries *Angewandte Chemie* 132 (16) 2020: pp. 6468 – 6473.
https://doi.org/10.1002/ange.201914972

7. **Wei, X., Zheng, D., Zhao, M., Chen, H., Fan, X., Gao, B., Gu, L., Guo, Y., Qin, J., Wei, J., Zhao, Y., Zhang, G.** Cross-Linked Polyphosphazene Hollow Nanosphere-Derived N/P-Doped Porous Carbon with Single Nonprecious Metal Atoms for the Oxygen Reduction Reaction *Angewandte Chemie International Edition* 59 (34) 2020: pp. 14639 – 14646.
https://doi.org/10.1002/anie.202006175

8. **Ren, J., Huang, Y., Zhu, H., Zhang, B., Zhu, H., Shen, S., Tan, G., Wu, F., He, H., Lan, S., Xia, X., Liu, Q.** Recent Progress on Mof-Derived Carbon Materials for Energy Storage *Carbon Energy* 2 (2) 2020: pp. 176 – 202.
https://doi.org/10.1002/cey2.44

9. **Khatib, M., Haick, H.** Sensors for Volatile Organic Compounds *ACS Nano* 16 (5) 2022: pp. 7080 – 7115.
https://doi.org/10.1021/acsnano.1c10827

10. **Weisskopf, L., Schulz, S., Garbeva, P.** Microbial Volatile Organic Compounds in Intra-Kingdom and Inter-Kingdom Interactions *Nature Reviews Microbiology* 19 (6) 2021: pp. 391 – 404.
https://doi.org/10.1038/s41579-020-00508-1

11. **Gu, S., Guenther, A., Faiola, C.** Effects of Anthropogenic and Biogenic Volatile Organic Compounds on Los Angeles Air Quality *Environmental Science & Technology* 55 (18) 2021: pp. 12191 – 12201.
https://doi.org/10.1021/acs.est.1c01481

12. **Matsagar, B.M., Yang, R.X., Dutta, S., Ok, Y.S., Wu, K.C.W.** Recent Progress in the Development of Biomass-Derived Nitrogen-Doped Porous Carbon *Journal of Materials Chemistry* A9 (7) 2021: pp. 3703 – 3728.
https://doi.org/10.1039/D0TA09706C

13. **Fu, R., Yu, C., Li, S., Yu, J., Wang, Z., Guo, W., Xie, Y., Yang, L., Liu, K., Ren, W., Qiu, J.** A Closed-Loop and Scalable Process for the Production of Biomass-Derived Superhydrophilic Carbon for Supercapacitors *Green Chemistry* 23 (9) 2021: pp. 3400 – 3409.
https://doi.org/10.1039/D1GC00670C

14. **Yang, W., Peng, D., Kimura, H., Zhang, X., Sun, X., Pashameah, R.A., Alzahrani, E., Wang, B., Guo, Z., Du, W., Hou, C.** Honeycomb-Like Nitrogen-Doped Porous Carbon Decorated with Co_3O_4 Nanoparticles for Superior Electrochemical Performance Pseudo-Capacitive Lithium Storage and Supercapacitors *Advanced Composites and Hybrid Materials* 5 (4) 2022: pp. 3146 – 3157.
https://doi.org/10.1007/s42114-022-00556-6

15. **Huo, S., Zhao, Y., Zong, M., Liang, B., Zhang, X., Khan, I.U., Song, X., Li, K.** Boosting Supercapacitor and Capacitive Deionization Performance of Hierarchically Porous Carbon by Polar Surface and Structural Engineering *Journal of Materials Chemistry* A8 (5) 2020: pp. 2505 – 2517.
https://doi.org/10.1039/C9TA12170F

16. **Ding, R., Chen, Q., Luo, Q., Zhou, L., Wang, Y., Zhang, Y., Fan, G.** Salt Template-Assisted in Situ Construction of Ru Nanoclusters and Porous Carbon: Excellent Catalysts toward Hydrogen Evolution, Ammonia-Borane Hydrolysis, and 4-Nitrophenol Reduction *Green Chemistry* 22 (3) 2020: pp. 835 – 842.
https://doi.org/10.1039/C9GC03986D

17. **Lu, T., Xu, X., Zhang, S., Pan, L., Wang, Y., Alshehri, S.M., Ahamad, T., Kim, M., Na, J., Hossain, M.S.A., Shapter, J.G., Yamauchi, Y.** High-Performance Capacitive Deionization by Lignocellulose-Derived Eco-Friendly Porous Carbon Materials *Bulletin of the Chemical Society of Japan* 93 (8) 2020: pp. 1014 – 1019.
https://doi.org/10.1246/bcsj.20200055

18. **Gong, Y., Li, D., Fu, Q., Zhang, Y., Pan, C.** Nitrogen Self-Doped Porous Carbon for High-Performance Supercapacitors *ACS Applied Energy Materials* 3 (2) 2020: pp. 1585 – 1592.
https://doi.org/10.1021/acsaem.9b02077

19. **Li, W., Guo, F., Wei, X., Du, Y., Chen, Y.** Preparation of Ni/c Porous Fibers Derived from Jute Fibers for High-Performance Microwave Absorption *RSC Advances* 10 (60) 2020: pp. 36644 – 36653.
https://doi.org/10.1039/d0ra06817a

20. **Li, Y., Li, X., Zhang, H., Xiang, Q.** Porous Graphitic Carbon Nitride for Solar Photocatalytic Applications *Nanoscale Horizons* 5 (5) 2020: pp. 765 – 786.
https://doi.org/10.1039/D0NH00046A

21. **Veerakumar, P., Sangili, A., Manavalan, S., Thanasekaran, P., Lin, K.C.** Research Progress on Porous Carbon Supported Metal/Metal Oxide Nanomaterials for Supercapacitor Electrode Applications *Industrial & Engineering Chemistry Research* 59 (14) 2020: pp. 6347 – 6374.
https://doi.org/10.1021/acs.iecr.9b06010

22. **Zhang, W., Tian, Y., He, H., Xu, L., Li, W., Zhao, D.** Recent Advances in the Synthesis of Hierarchically Mesoporous Tio_2 Materials for Energy and Environmental Applications *National Science Review* 7 (11) 2020: pp. 1702 – 1725.
https://doi.org/10.1093/nsr/nwaa021

23. **Cai, G., Yan, P., Zhang, L., Zhou, H.C., Jiang, H.L.** Metal–Organic Framework-Based Hierarchically Porous Materials: Synthesis and Applications *Chemical Reviews* 121 (20) 2021: pp. 12278 – 12326.
https://doi.org/10.1021/acs.chemrev.1c00243

24. **Liu, Y., Liu, L., Wang, Y.** A Critical Review on Removal of Gaseous Pollutants Using Sulfate Radical-Based Advanced Oxidation Technologies *Environmental Science & Technology* 55 (14) 2021: pp. 9691 – 9710. https://doi.org/10.1021/acs.est.1c01531

25. **Lu, T., Cui, J., Qu, Q., Wang, Y., Zhang, J., Xiong, R., Ma, W., Huang, C.** Multistructured Electrospun Nanofibers for Air Filtration: a Review *ACS Applied Materials & Interfaces* 13 (20) 2021: pp. 23293 – 23313. https://doi.org/10.1021/acsami.1c06520

26. **Bolan, N., Hoang, S.A., Beiyuan, J., Gupta, S., Hou, D., Karakoti, A., Joseph, S., Jung, S., Kim, K.H.** Multifunctional Applications of Biochar Beyond Carbon Storage *International Materials Reviews* 67 (2) 2022: pp. 150 – 200. https://doi.org/10.1080/09506608.2021.1922047

27. **Anfar, Z., Ait Ahsaine, H., Zbair, M., Amedlous, A., Ait El Fakir, A., Jada, A., El Alem, N.** Recent Trends on Numerical Investigations of Response Surface Methodology for Pollutants Adsorption onto Activated Carbon Materials: a Review *Critical Reviews in Environmental Science and Technology* 50 (10) 2020: pp. 1043 – 1084. https://doi.org/10.1080/10643389.2019.1642835